SIAM J. SCI. COMPUT.
Vol. 37, No. 2, pp. B261–B282

A TIME-SPLITTING FINITE-ELEMENT STABLE APPROXIMATION FOR THE ERICKSEN–LESLIE EQUATIONS*

R. C. CABRALES†, F. GUILLÉN-GONZÁLEZ‡, AND J. V. GUTIÉRREZ-SANTACREU§

Abstract. In this paper we propose an unconditional energy-stable time-splitting finite-element scheme for approximating the Ericksen–Leslie equations governing the flow of nematic liquid crystals. These equations are to be solved for a velocity vector field and a scalar pressure as well as a director vector field representing the direction along which the molecules of the liquid crystal are oriented. The algorithm is designed at two levels. First, at the variational level, the velocity, pressure, and director are computed separately, but the director field has to be computed together with an auxiliary variable (associated to the equilibrium equation for the director) in order to deduce a priori energy estimates. Second, at the algebraic level, one can avoid computing such an auxiliary variable if this is approximated by a piecewise constant finite-element space. Therefore, these two steps give rise to a numerical algorithm that computes separately only the primary variables: velocity, pressure, and director vector. Moreover, we will use a pressure stabilization technique that allows a stable equal-order interpolation for the velocity and the pressure. Finally, some numerical simulations are performed in order to show the robustness and efficiency of the proposed numerical scheme and its accuracy.

Key words. nematic liquid crystal, finite elements, projection method, time-splitting method, stabilized methods

AMS subject classifications. 35Q35, 65M60, 76A15

DOI. 10.1137/140960979

1. Introduction.

In recent years, there has been great interest in the numerical approximation of liquid crystal flows. The reason for this is that liquid crystals are not easy to study from experimental observations due to the effect of boundary conditions of the confining geometries. Thus, numerical simulations may allow a clear insight into the behavior of liquid crystals and the understanding of their underlying physical properties. For instance, numerical simulations contribute to improving the design of practical devices.

Liquid crystals are materials that show intermediate transitions between solid and liquid phases, called *mesophases*. This means that liquid crystals combine features of both isotropic liquids and crystalline solids. These mesophases are due, in part, to the fact that liquid crystals are made of macromolecules of similar shape and size, which are commonly represented as rods or plates.

*Submitted to the journal's Computational Methods in Science and Engineering section March 14, 2014; accepted for publication (in revised form) January 13, 2015; published electronically March 11, 2015.

http://www.siam.org/journals/sisc/37-2/96097.html

†Departamento de Ciencias Básicas, Universidad del Bío-Bío, Casilla 447, Chillán, Chile (roberto.cabrales@gmail.com). This author's work was partially supported under grants GI 121909/C, Universidad del Bío-Bío, Chile; Fondecyt 1140074, Chile; and MTM2012-32325, Ministerio de Economía y Competitividad, Spain.

‡Dpto. E.D.A.N., Universidad de Sevilla, 41080 Sevilla, Spain (guillen@us.es). This author's work was partially supported by Ministerio de Economía y Competitividad under grant MTM2012-32325, Spain.

§Dpto. de Matemática Aplicada I, E. T. S. I. Informática, Universidad de Sevilla, Avda. Reina Mercedes, s/n, 41012 Sevilla, Spain (juanvi@us.es). This author's work was partially supported by Ministerio de Economía y Competitividad and Ministerio de Educación under grants MTM2012-32325 and JC2011-418, Spain.

The mathematical theory describes liquid crystals based on the different degrees of positional and orientational ordering of their molecules. Thus, the position order alludes to the relative position of the molecules, while the orientation order refers to the fact that the molecules tend to be locally aligned toward a certain preferred direction. Such a direction is described by a unit vector along the molecule if rod-shaped or perpendicular to the molecule if plate-shaped that measures the mean values of alignments.

The simplest phase of liquid crystals, called *nematic*, possesses an orientational ordering but not a positional ordering. That is, the molecules flow freely as in a disordered isotropic liquid phase while tending to be orientated along a direction which can be manipulated with mechanical (boundary conditions), magnetic, or electric forces.

The simplest phenomenological description of spatial configurations in nematic liquid crystals is the Oseen–Frank theory [31, 15]. This approach consists in modeling equilibrium states as minima of a free energy, depending on the director vector $\boldsymbol{d}$, which is set up through symmetry and invariance principles to capture some properties observed from experiments. In its most basic form, the free energy functional is given by

$$E(\boldsymbol{d}) = K \int_\Omega |\nabla \boldsymbol{d}|^2,$$

where $K > 0$ is an elastic constant. Upon minimizing this energy subject to the sphere constraint $|\boldsymbol{d}| = 1$, the following optimality system appears:

$$-\Delta \boldsymbol{d} - |\nabla \boldsymbol{d}|^2 \boldsymbol{d} = \boldsymbol{0} \quad \text{in } \Omega.$$

The defect points or singularities in liquid crystals are regions where the anisotropic properties of molecules are broken. That is, the liquid crystal behaves in local zones as an isotropic fluid, where the director field cannot be defined. Mathematically, these defects are modeled by $|\boldsymbol{d}| = 0$. The limitation in the Oseen–Frank theory relies on the fact that it can explain only point defects in liquid crystal materials but not the more complicated line and surface defects that are also observed experimentally. One way of inducing defect points is with the help of the boundary conditions.

The motion of defect points in liquid crystals can be studied via the long-time behavior of the harmonic map flow for which it is also interesting to incorporate the influence of the velocity. On the contrary, in many situations, the anisotropic local orientation of the director field influences the stress tensors that govern the fluid velocity. The hydrodynamic theory of nematic liquid crystals was established by Ericksen [13, 12] and Leslie [22, 21]. The fundamental system consists of a set of fully coupled, macroscopic equations, which contains the Oseen–Frank elastic theory governing the steady state of equilibrium solutions.

The remaining part of this paper is organized as follows. Section 2 starts by establishing some notation used throughout this paper. Then we follow with the differential formulation of the Ericksen–Leslie and Ginzburg–Landau equations. To end the section, we sum up the main contributions on the finite-element approximation of the Ginzburg–Landau equations. In section 3 we give some shorthand notation for finite-element spaces in order to be able to define the projection time-stepping algorithm and give a brief introduction of some key ideas leading to the proposed method. Next, in section 4, we prove a priori estimates for the algorithm. Section 5 is devoted to some implementation improvements at the algebraic level and validating the scheme with some numerical simulations.

2. Statement of the problem. Let $\Omega \subset \mathbb{R}^M, M = 2, 3$, be any bounded open set with boundary $\partial\Omega$. For $1 \le p \le \infty$, $L^p(\Omega)$ denotes the space of pth-power integrable real-valued functions defined on Ω for the Lebesgue measure. This space is a Banach space endowed with the norm $\|v\|_{L^p(\Omega)} = (\int_\Omega |v(\boldsymbol{x})|^p \,\mathrm{d}\boldsymbol{x})^{1/p}$ for $1 \le p < \infty$ or $\|v\|_{L^\infty(\Omega)} = \operatorname{ess\,sup}_{\boldsymbol{x}\in\Omega} |v(\boldsymbol{x})|$ for $p = \infty$. In particular, $L^2(\Omega)$ is a Hilbert space with the inner product

$$(u, v) = \int_\Omega u(\boldsymbol{x})v(\boldsymbol{x})\mathrm{d}\boldsymbol{x},$$

and its norm is simply denoted by $\|\cdot\|$. For m a nonnegative integer, we define the classical Sobolev spaces as

$$H^m(\Omega) = \{v \in L^2(\Omega)\,;\, \partial^k v \in L^2(\Omega)\ \forall\, |k| \le m\},$$

associated to the norm

$$\|v\|_{H^m(\Omega)} = \left[\sum_{0\le|k|\le m} \|\partial^k v\|^2\right]^{\frac{1}{2}},$$

where $k = (k_1, \ldots, k_M) \in \mathbb{N}^M$ is a multi-index and $|k| = \sum_{i=1}^M k_i$, which is a Hilbert space with the obvious inner product. We will use boldface letters for spaces of vector functions and their elements, e.g., $\boldsymbol{L}^2(\Omega)$ in place of $L^2(\Omega)^M$.

Let $\mathcal{D}(\Omega)$ be the space of infinitely times differentiable functions with compact support on Ω. The closure of $\mathcal{D}(\Omega)$ in $H^m(\Omega)$ is denoted by $H_0^m(\Omega)$. We will also make use of the following space of vector fields:

$$\boldsymbol{\mathcal{V}} = \{\boldsymbol{v} \in \boldsymbol{\mathcal{D}}(\Omega) : \nabla \cdot \boldsymbol{v} = 0 \text{ in } \Omega\},$$

where $\nabla \cdot \boldsymbol{u} = \sum_{i=1}^M \partial_i u_i$ is the divergence operator. We denote by $\boldsymbol{H}$ and $\boldsymbol{V}$ the closures of $\boldsymbol{\mathcal{V}}$ in the $\boldsymbol{L}^2(\Omega)$- and $\boldsymbol{H}^1(\Omega)$-norm, respectively, which are characterized by (see [36])

$$\boldsymbol{H} = \{\boldsymbol{u} \in \boldsymbol{L}^2(\Omega) : \nabla \cdot \boldsymbol{u} = 0 \text{ in } \Omega,\ \boldsymbol{u} \cdot \boldsymbol{n} = 0 \text{ on } \partial\Omega\},$$
$$\boldsymbol{V} = \{\boldsymbol{u} \in \boldsymbol{H}^1(\Omega) : \nabla \cdot \boldsymbol{u} = 0 \text{ in } \Omega,\ \boldsymbol{u} = \boldsymbol{0} \text{ on } \partial\Omega\},$$

where $\boldsymbol{n}$ is the outward normal to Ω on $\partial\Omega$. This characterization is valid for Ω being Lipschitzian. Finally, we consider

$$L_0^2(\Omega) = \left\{p \in L^2(\Omega) :\ \int_\Omega p(\boldsymbol{x})\, d\boldsymbol{x} = 0\right\}.$$

2.1. The Ericksen–Leslie problem. Let $T > 0$ be a fixed time. We will use the notation $Q = \Omega \times (0, T)$ and $\Sigma = \partial\Omega \times (0, T)$. The Ericksen–Leslie equations are written as

$$\begin{cases} \partial_t \boldsymbol{d} + (\boldsymbol{u} \cdot \nabla)\boldsymbol{d} - \gamma\Delta\boldsymbol{d} - \gamma|\nabla\boldsymbol{d}|^2\boldsymbol{d} = \boldsymbol{0} & \text{in } Q, \quad \text{(2.1a)} \\ |\boldsymbol{d}| = 1 & \text{in } Q, \quad \text{(2.1b)} \\ \partial_t \boldsymbol{u} + (\boldsymbol{u} \cdot \nabla)\boldsymbol{u} - \nu\Delta\boldsymbol{u} + \nabla p + \lambda\nabla \cdot ((\nabla\boldsymbol{d})^T\nabla\boldsymbol{d}) = \boldsymbol{0} & \text{in } Q, \quad \text{(2.1c)} \\ \nabla\cdot \boldsymbol{u} = 0 & \text{in } Q, \quad \text{(2.1d)} \end{cases}$$

where $\boldsymbol{u} : \overline{Q} \to \mathbb{R}^M$ is the fluid velocity, $p : \overline{Q} \to \mathbb{R}$ is the fluid pressure, and $\boldsymbol{d} : \overline{Q} \to \mathbb{R}^M$ is the orientation of the molecules. The parameter $\nu > 0$ is a constant depending on the fluid viscosity, $\lambda > 0$ is an elasticity constant, and $\gamma > 0$ is a relaxation time constant. The operators involved in system (2.1) are described as follows. The Laplacian operator $\Delta \boldsymbol{u} = \sum_{i=1}^{M} \partial_{ii} \boldsymbol{u}$; the convective operator $(\boldsymbol{u} \cdot \nabla)\boldsymbol{w} = \sum_{i=1}^{M} u_i \partial_i \boldsymbol{w}$. Moreover, $(\nabla \boldsymbol{d})^T$ denotes the transposed matrix of $\nabla \boldsymbol{d} = (\partial_j d_i)_{i,j}$, and $|\boldsymbol{d}| = |\boldsymbol{d}(\boldsymbol{x}, t)|$ is the Euclidean norm in $\mathbb{R}^M$.

The system (2.1) provides a phenomenological description for the hydrodynamics of nematic liquid crystals from the macroscopic point of view. It was reduced to essentials by Lin [23] from the fundamental set of fully coupled, macroscopic equations derived by Ericksen [13, 12] and Leslie [22, 21], which contains the Oseen–Frank elastic energy governing the steady state as equilibrium solutions.

Equation (2.1a) models the conservation of the angular momentum; in particular, together with (2.1b), it is a convective harmonic heat map flow equation into spheres. The latter indicates that $\boldsymbol{d}$ is not a state variable; it only describes the orientation of the nematic liquid crystal molecules. Equations (2.1c) and (2.1d) are the Navier–Stokes equations related to the conservation of the linear momentum. The molecules add (elastic) stress to the fluid via the term $\lambda \nabla \cdot ((\nabla \boldsymbol{d})^T \nabla \boldsymbol{d})$, and the fluid transports the molecules via the term $(\boldsymbol{u} \cdot \nabla)\boldsymbol{d}$.

To these equations we will add homogeneous Dirichlet conditions for the velocity field and homogeneous Neumann boundary conditions for the director field,

$$\boldsymbol{u}(\boldsymbol{x}, t) = \boldsymbol{0}, \quad \partial_{\boldsymbol{n}} \boldsymbol{d}(\boldsymbol{x}, t) = \boldsymbol{0} \quad \text{for } (\boldsymbol{x}, t) \in \Sigma, \tag{2.2}$$

and the initial conditions

$$\boldsymbol{d}(\boldsymbol{x}, 0) = \boldsymbol{d}_0(\boldsymbol{x}), \qquad \boldsymbol{u}(\boldsymbol{x}, 0) = \boldsymbol{u}_0(\boldsymbol{x}) \quad \text{for } \boldsymbol{x} \in \Omega. \tag{2.3}$$

Here $\boldsymbol{u}_0 : \Omega \to \mathbb{R}^M$, with $\boldsymbol{u}_0 \in \boldsymbol{H}$, and $\boldsymbol{d}_0 : \Omega \to \mathbb{R}^M$, with $\boldsymbol{d}_0 \in \boldsymbol{H}^1(\Omega)$ satisfying $|\boldsymbol{d}_0| = 1$ in Ω, are given functions.

The following energy law for system (2.1) holds under some regularity assumptions for $\boldsymbol{u}$ and $\boldsymbol{d}$:

$$\frac{d}{dt}\left(\frac{1}{2}\|\boldsymbol{u}\|^2 + \frac{\lambda}{2}\|\nabla \boldsymbol{d}\|^2\right) + \nu\|\nabla \boldsymbol{u}\|^2 + \lambda\gamma\|\Delta \boldsymbol{d} + |\nabla \boldsymbol{d}|^2 \boldsymbol{d}\|^2 = 0. \tag{2.4}$$

However, it requires that $\boldsymbol{d}$ must have the unit length, i.e., $|\boldsymbol{d}| = 1$ almost everywhere in Q. It makes system (2.1) difficult to manage from the numerical point of view since the satisfaction of the sphere constraint at the nodes is not implied at any other points via interpolation. For this reason, two approaches have been considered for dealing with it: a penalty method and a saddle-point method. These techniques provide numerical schemes with an associated energy law without the need of satisfying the sphere constraint for $\boldsymbol{d}$. The penalty method has been intensively studied compared to the saddle-point strategy since the latter makes it more challenging to perform the numerical analysis rigorously. The difficulty lies in proving an inf-sup condition for the Lagrangian multiplier related to the sphere constraint. In order to hold an inf-sup condition [20], a stronger regularity than that provided by (2.4) is needed; therefore establishing an inf-sup condition under the regularity stemming from (2.1) is still an interesting, open problem.

2.2. A Ginzburg–Landau penalized problem. A general penalty version of system (2.1) to enforce the sphere constraint reads as

$$\begin{cases} \partial_t \boldsymbol{d} + (\boldsymbol{u}\cdot\nabla)\boldsymbol{d} + \gamma\left(\frac{1}{\varepsilon^2}\boldsymbol{f}(\boldsymbol{d}) - \Delta\boldsymbol{d}\right) = \boldsymbol{0} & \text{in } Q, \quad (2.5a)\\ \partial_t \boldsymbol{u} + (\boldsymbol{u}\cdot\nabla)\boldsymbol{u} - \nu\Delta\boldsymbol{u} + \nabla p + \lambda\nabla\cdot((\nabla\boldsymbol{d})^T\nabla\boldsymbol{d}) = \boldsymbol{0} & \text{in } Q, \quad (2.5b)\\ \nabla\cdot\boldsymbol{u} = 0 & \text{in } Q, \quad (2.5c) \end{cases}$$

where $\boldsymbol{f}(\boldsymbol{d})$ is the penalty function related to the constraint $|\boldsymbol{d}| = 1$, and $\varepsilon > 0$ is the penalty parameter. It is important to select $\boldsymbol{f}(\boldsymbol{d})$ to be the gradient of a scalar-valued function $F(\boldsymbol{d})$, i.e., $\boldsymbol{f}(\boldsymbol{d}) = \nabla_{\boldsymbol{d}} F(\boldsymbol{d})$ for all $\boldsymbol{d} \in \mathbb{R}^M$. This penalty term can also be physically meaningful and represents a possible extensibility of molecules. Let us define a truncated potential

$$F(\boldsymbol{d}) = \begin{cases} \frac{1}{4}(|\boldsymbol{d}|^2 - 1)^2 & \text{if } |\boldsymbol{d}| \le 1,\\ (|\boldsymbol{d}| - 1)^2 & \text{if } |\boldsymbol{d}| > 1; \end{cases} \quad (2.6)$$

hence

$$\nabla_{\boldsymbol{d}} F(\boldsymbol{d}) = \boldsymbol{f}(\boldsymbol{d}) = \begin{cases} (|\boldsymbol{d}|^2 - 1)\boldsymbol{d} & \text{if } |\boldsymbol{d}| \le 1,\\ 2(|\boldsymbol{d}| - 1)\dfrac{\boldsymbol{d}}{|\boldsymbol{d}|} & \text{if } |\boldsymbol{d}| > 1. \end{cases} \quad (2.7)$$

The virtue of system (2.5) is that its solutions satisfy an energy law without assuming any restriction on $\boldsymbol{d}$ as was mentioned above. We give here a sketch of the proof of the energy estimate obtained in [6] based on that of [24] in order to have a clear picture of how our numerical scheme is designed. First, note that

$$\lambda\nabla\cdot((\nabla\boldsymbol{d})^T\nabla\boldsymbol{d}) = \lambda\nabla\left(\frac{1}{2}|\nabla\boldsymbol{d}|^2 + \frac{1}{\varepsilon^2}F(\boldsymbol{d})\right) - \lambda(\nabla\boldsymbol{d})^T\left(-\Delta\boldsymbol{d} + \frac{1}{\varepsilon^2}\boldsymbol{f}(\boldsymbol{d})\right)$$

and

$$[(\boldsymbol{u}\cdot\nabla)\boldsymbol{d}]\cdot\left(-\Delta\boldsymbol{d} + \frac{1}{\varepsilon^2}\boldsymbol{f}(\boldsymbol{d})\right) = (\nabla\boldsymbol{d})^T\left(-\Delta\boldsymbol{d} + \frac{1}{\varepsilon^2}\boldsymbol{f}(\boldsymbol{d})\right)\cdot\boldsymbol{u}.$$

Next, multiplying (2.5a) and (2.5b) by $\lambda(-\Delta\boldsymbol{d} + \frac{1}{\varepsilon^2}\boldsymbol{f}(\boldsymbol{d}))$ and $\boldsymbol{u}$, respectively, and integrating over Ω, we obtain, after some integrations by parts,

$$\frac{d}{dt}\mathcal{E}(\boldsymbol{u},\boldsymbol{d}) + \nu\|\nabla\boldsymbol{u}\|^2 + \lambda\gamma\left\|-\Delta\boldsymbol{d} + \frac{1}{\varepsilon^2}\boldsymbol{f}(\boldsymbol{d})\right\|^2 = 0, \quad (2.8)$$

where

$$\mathcal{E}(\boldsymbol{u},\boldsymbol{d}) = \frac{1}{2}\|\boldsymbol{u}\|^2 + \frac{\lambda}{2}\|\nabla\boldsymbol{d}\|^2 + \frac{\lambda}{\varepsilon^2}\int_\Omega F(\boldsymbol{d}) \quad (2.9)$$

represents the total energy involving the model, which consists of the kinetic energy $\frac{1}{2}\|\boldsymbol{u}\|^2$, the elastic energy $\frac{\lambda}{2}\|\nabla\boldsymbol{d}\|^2$, and the penalty energy $\frac{\lambda}{\varepsilon^2}\int_\Omega F(\boldsymbol{d})$.

System (2.5) can be viewed as being a regularization of the Ericksen–Leslie equations (2.1) since one can prove the extra regularity estimate [6]:

$$\int_0^T \|\Delta\boldsymbol{d}(t)\|^2\,dt \le \frac{C}{\varepsilon^2}.$$

Obviously, such an estimate has no meaning as the penalization parameter ε goes to zero.

2.3. Known results. We discuss briefly the previous numerical schemes applied to the Ginzburg–Landau problem. The first two numerical schemes for problem (2.5) were the works of Liu and Walkington [28, 29]. The former used an implicit Euler time-stepping scheme together with LBB-stable finite elements for the velocity and pressure and Hermite bicubic C^1–finite elements for the director. Nevertheless, the algorithm turned out to be computationally expensive due to the number of degrees of freedom involving in the resolution together with the fact that the performance was not an easy task because of the set of finite-element basis functions connecting derivatives up to second order. The latter scheme used the same time discretization but took advantage of using the auxiliary variable $\boldsymbol{w} = \nabla \boldsymbol{d}$ in order to rule out the complexity of using C^1–finite elements, even though the number of new unknowns made the algorithm inefficient for large-scale simulations. Afterwards came the work of Lin and Liu [26], who utilized a time-stepping semiexplicit Euler algorithm, where the stress tensor $\nabla \cdot ((\nabla \boldsymbol{d})^T \nabla \boldsymbol{d})$ was explicitly discretized, separating the computation of the velocity and pressure from that of the director. Girault and Guillén-González [16] introduced the auxiliary variable $\boldsymbol{w} = -\Delta \boldsymbol{d}$ in order to design a semiexplicit Euler scheme where the Ginzburg–Landau function was explicitly discretized. It is clear that the use of the Laplacian operator in place of the gradient operator as in [29] reduced considerably the number of global unknowns. One common feature of all of these numerical schemes described above is that no discrete energy law equivalent to (2.8) was proved, and hence a priori estimates independent of the penalty parameter ε could not be deduced.

To the best of our knowledge, the only numerical scheme that preserved a discrete version of (2.8) made use of the auxiliary variable $\boldsymbol{w} = -\Delta \boldsymbol{d} + \frac{1}{\varepsilon^2} \boldsymbol{f}(\boldsymbol{d})$ along with an explicit-concave, implicit-convex time discretization of the Ginzburg–Landau penalty function $\boldsymbol{f}(\boldsymbol{d}) = (|\boldsymbol{d}|^2 - 1)\boldsymbol{d}$ (see [6]) leading to a nonlinear scheme. Following the same ideas as in [6], a linear scheme was developed in [18] by using a fully explicit time integration of the potential term, either truncated or not. The algorithm presented in this paper starts from [18].

Recently, in [3], a saddle-point strategy was suggested for both the Ericksen–Leslie and the Ginzburg–Laundau equations resulting in numerical algorithms which maintain an energy equality comparable to (2.8). The reader is referred to [4] for a survey of numerical methods on the Ginzburg–Landau approximation.

2.4. The main contribution of this paper. An important observation concerning numerical schemes which embody an energy law from system (2.5) is that the time integration couples all the unknowns; therefore, the computational work required to solve a time step makes them extremely expensive. Thus, the difficulty in designing an efficient numerical approximation for system (2.5) lies in choosing a time discretization that, as well as providing energy estimates independent of the penalty parameter ε, decouples all the variables being computed. Observe that problem (2.5) consists of the Navier–Stokes equations for velocity and pressure with an extra "elastic" stress tensor, and a convective harmonic map heat flow system to govern the dynamics of the director field.

Projection time-stepping strategies are used in the context of Navier–Stokes as efficient time-splitting integrations. The starting point of most projection time-stepping methods is the Chorin–Temam algorithm [9, 35], which decouples the computation of the velocity field from that of the pressure, separating the incompressibility constraint from the momentum equation. However, in order to apply such a method to the Ginzburg–Landau equations, we need some additional strategies so that the

computation of the director vector can be also segregated. The same difficulty arises in the context of magnetohydrodynamics (MHD) fluids for which Armero and Simo [1] designed an algorithm which decoupled the computation of the velocity field from that of the magnetic field. We refer the reader to [5], where the ideas of Chorin and Temam are combined with those of Armero and Simo for the MHD equations. It is in this spirit that the algorithm presented in [30] is designed for a triphasic Navier–Stokes/Cahn–Hilliard problem, decoupling the Navier–Stokes subproblem from the Cahn–Hilliard one.

The goal of this paper is then to extend these types of strategies for developing a numerical scheme for (2.5) which is linear, uses low-order finite elements, decouples the angular, the momentum, and the incompressibility equations, preserves a discrete energy law without requiring a relation between the discretization parameters and the penalty parameter, does not need any additional variable, and avoids an inf-sup condition for velocity and pressure.

3. Finite element approximation.

3.1. Preliminaries. Herein we introduce the hypotheses that will be required throughout this paper.

- (H1) Let Ω be a bounded domain of $\mathbb{R}^M$ with a polygonal or polyhedral Lipschitz-continuous boundary.
- (H2) Let $\{\mathcal{T}_h\}_{h>0}$ be a family of regular, quasi-uniform triangulations of $\overline{\Omega}$ made up of triangles in two dimensions and tetrahedra in three dimensions, so that $\overline{\Omega} = \cup_{K\in\mathcal{T}_h} K$.
- (H3) Conforming finite-element spaces associated with $\mathcal{T}_h$ are assumed.
- (H4) We suppose that $(\boldsymbol{u}_0, \boldsymbol{d}_0) \in \boldsymbol{H} \times \boldsymbol{H}^1(\Omega)$ with $|\boldsymbol{d}_0| = 1$ a.e. in Ω.

Hypothesis (H3) is extremely flexible and allows equal-order finite-element spaces for velocity and pressure. In particular, let $\mathcal{P}_1(K)$ be the set of linear polynomials on K. Thus the space of continuous, piecewise polynomial functions associated to $\mathcal{T}_h$ is denoted as

$$X_h = \left\{ v_h \in C^0(\overline{\Omega}) \ : \ v_h|_K \in \mathcal{P}_1(K) \ \forall\, K \in \mathcal{T}_h \right\},$$

and the set of piecewise constant functions as

$$Y_h = \{ w_h \in L^\infty(\Omega) \ : \ w_h|_K \in \mathbb{R} \ \forall\, K \in \mathcal{T}_h \}.$$

We choose the continuous finite-element spaces

$$\boldsymbol{D}_h = \boldsymbol{X}_h, \quad \boldsymbol{V}_h = \boldsymbol{X}_h \cap \boldsymbol{H}_0^1(\Omega), \quad \text{and} \quad P_h = X_h \cap L_0^2(\Omega)$$

for approximating the director, the velocity, and the pressure, respectively. Additionally, we select the extra discontinuous finite-element $\boldsymbol{W}_h = \boldsymbol{Y}_h$ to be the space for an auxiliary variable related with the vector director.

Observe that our choice of the finite-element spaces for velocity and pressure does not satisfy the discrete inf-sup condition

$$\|p_h\|_{L_0^2(\Omega)} \leq \alpha \sup_{\boldsymbol{v}_h \in \boldsymbol{V}_h \setminus \{0\}} \frac{(q_h, \nabla \cdot \boldsymbol{v}_h)}{\|\boldsymbol{v}_h\|_{H^1(\Omega)}} \quad \forall\, p_h \in P_h, \tag{3.1}$$

for $\alpha > 0$ independent of h.

The following proposition is concerned with an interpolation operator I_h associated with the space $\boldsymbol{D}_h$. In fact, we can think of I_h as the Scott–Zhang interpolation operator; see [33].

PROPOSITION 3.1. *Assuming hypotheses* (H1)–(H3)*, there exists* $I_h : \boldsymbol{H}^1(\Omega) \to \boldsymbol{D}_h$*, an interpolation operator satisfying*

$$\|\boldsymbol{d} - I_h\boldsymbol{d}\| \le C_{app}\, h\|\nabla \boldsymbol{d}\| \quad \forall\, \boldsymbol{d} \in \boldsymbol{H}^1(\Omega) \tag{3.2}$$

and

$$\|I_h\boldsymbol{d}\|_{\boldsymbol{L}^\infty(\Omega)} \le C_{sta}\|\boldsymbol{d}\|_{\boldsymbol{L}^\infty(\Omega)} \quad \forall\, \boldsymbol{d} \in \boldsymbol{L}^\infty(\Omega), \tag{3.3}$$

$$\|I_h\boldsymbol{d}\|_{\boldsymbol{H}^1(\Omega)} \le C_{sta}\|\boldsymbol{d}\|_{\boldsymbol{H}^1(\Omega)} \quad \forall\, \boldsymbol{d} \in \boldsymbol{H}^1(\Omega), \tag{3.4}$$

where $C_{app} > 0$ *and* $C_{sta} > 0$ *are constants independent of* h*.*

3.2. The time-stepping method. We consider the following time-splitting finite-element method for approximating (2.5) based on the nonincremental projection technique.

Let $(\boldsymbol{d}_h^n, \boldsymbol{u}_h^n, p_h^n) \in \boldsymbol{D}_h \times \boldsymbol{V}_h \times P_h$ be given. For $n+1$, do the following steps:

1. Find $(\boldsymbol{d}_h^{n+1}, \boldsymbol{w}_h^{n+1}) \in \boldsymbol{D}_h \times \boldsymbol{W}_h$ satisfying

$$\left(\frac{\boldsymbol{d}_h^{n+1} - \boldsymbol{d}_h^n}{k}, \bar{\boldsymbol{w}}_h\right) + ((\widehat{\boldsymbol{u}}_h \cdot \nabla)\boldsymbol{d}_h^n, \bar{\boldsymbol{w}}_h) + \gamma(\boldsymbol{w}_h^{n+1}, \bar{\boldsymbol{w}}_h) = 0, \tag{3.5a}$$

$$\begin{aligned}(\nabla \boldsymbol{d}_h^{n+1}, \nabla \bar{\boldsymbol{d}}_h) + \frac{1}{\varepsilon^2}(\boldsymbol{f}(\boldsymbol{d}_h^n), \bar{\boldsymbol{d}}_h) \\ + \frac{H_F}{2\varepsilon^2}(\boldsymbol{d}_h^{n+1} - \boldsymbol{d}_h^n, \bar{\boldsymbol{d}}_h) - (\boldsymbol{w}_h^{n+1}, \bar{\boldsymbol{d}}_h) = 0\end{aligned} \tag{3.5b}$$

for all $(\bar{\boldsymbol{d}}_h, \bar{\boldsymbol{w}}_h) \in \boldsymbol{D}_h \times \boldsymbol{W}_h$, where

$$\widehat{\boldsymbol{u}}_h = \boldsymbol{u}_h^n - k\nabla p_h^n + \lambda\, k(\nabla \boldsymbol{d}_h^n)^T \boldsymbol{w}_h^{n+1} \tag{3.6}$$

and $H_F > 0$ is a bound of the L^∞-norm of the Hessian matrix associated to $F(\boldsymbol{d})$. For instance,

$$H_F := (M3^2 + (M^2 - M)2^2)^{1/2} \tag{3.7}$$

with M being the space dimension (see the proof of Lemma 4.1).

2. Find $\boldsymbol{u}_n^{n+1} \in \boldsymbol{V}_h$ satisfying

$$\begin{aligned}\left(\frac{\boldsymbol{u}_h^{n+1} - \boldsymbol{u}_h^n}{k}, \bar{\boldsymbol{u}}_h\right) + c(\boldsymbol{u}_h^n, \boldsymbol{u}_h^{n+1}, \bar{\boldsymbol{u}}_h) + \nu(\nabla \boldsymbol{u}_h^{n+1}, \nabla \bar{\boldsymbol{u}}_h) \\ + (\nabla p_h^n, \bar{\boldsymbol{u}}_h) - \lambda((\nabla \boldsymbol{d}_h^n)^T \boldsymbol{w}_h^{n+1}, \bar{\boldsymbol{u}}_h) = 0\end{aligned} \tag{3.8}$$

for all $\bar{\boldsymbol{u}}_h \in \boldsymbol{V}_h$.

3. Find $p_h^{n+1} \in P_h$ satisfying

$$k(\nabla p_h^{n+1}, \nabla \bar{p}_h) + j(p_h^{n+1}, \bar{p}_h) = -(\nabla \cdot \boldsymbol{u}_h^{n+1}, \bar{p}_h) \tag{3.9}$$

for all $\bar{p}_h \in P_h$, with

$$j(p_h^{n+1}, \bar{p}_h) = \frac{S}{\nu}(p_h^{n+1} - \Pi_0(p_h^{n+1}), \bar{p}_h - \Pi_0(\bar{p}_h)), \tag{3.10}$$

where S is an algorithmic constant and Π_0 is the L^2-orthogonal projection operator onto Y_h, which is a piecewise constant finite-element space.

To ensure the skew-symmetry of the trilinear convective term in (3.8), we have defined

$$c(\boldsymbol{u}_h, \boldsymbol{v}_h, \boldsymbol{w}_h) = ((\boldsymbol{u}_h \cdot \nabla)\boldsymbol{v}_h, \boldsymbol{w}_h) + \frac{1}{2}(\nabla \cdot \boldsymbol{u}_h, \boldsymbol{v}_h \cdot \boldsymbol{w}_h)$$

for all $\boldsymbol{u}_h, \boldsymbol{v}_h, \boldsymbol{w}_h \in \boldsymbol{V}_h$. Thus $c(\boldsymbol{u}_h, \boldsymbol{v}_h, \boldsymbol{v}_h) = 0$ for all $\boldsymbol{u}_h, \boldsymbol{v}_h \in \boldsymbol{V}_h$.

It is important to mention that we use the version of the nonincremental projection method to design scheme (3.5)–(3.10) where the end-of-step velocity has been eliminated.

The idea for the stabilization term $j(\cdot,\cdot)$ in (3.10) is to penalize the difference between the pressure and its projection onto the space of piecewise constant functions Y_h. This stabilization technique was proposed for the Stokes problem in [11]. The stabilization term $j(\cdot,\cdot)$ was inspired by the fact that the pressure stability provided by the crude projection time-stepping method depends on the time step k so that loss of pressure stability is expected when k is considerably small. The reader can refer to [8] for a general description of this stabilization technique. See also [2] for a stabilization using a Scott–Zhang projection operator.

It is good to point out that scheme (3.5)–(3.10) decouples the computation of the pair $(\boldsymbol{d}_h^{n+1}, \boldsymbol{w}_h^{n+1})$, the velocity $\boldsymbol{u}_h^{n+1}$, and the pressure p_h^{n+1}. The auxiliary variable $\boldsymbol{w}_h^{n+1}$ is introduced only to help us prove a priori energy estimates. The condensation of the degrees of freedom of $\boldsymbol{w}_h^{n+1}$ will be treated in detail in section 5 when we set up the algebraic version for (3.5).

For suitable initial approximations $(\boldsymbol{u}_{0h}, \boldsymbol{d}_{0h})$ of $(\boldsymbol{u}_0, \boldsymbol{d}_0)$, we consider $\boldsymbol{d}_{0h} \in \boldsymbol{D}_h$ such that

$$\boldsymbol{d}_{0h} = I_h \boldsymbol{d}_0 \tag{3.11}$$

and $(\boldsymbol{u}_{0h}, p_{0h}) \in \boldsymbol{V}_h \times P_h$ such that

$$\begin{cases} (\boldsymbol{u}_{0h}, \bar{\boldsymbol{u}}_h) + (\nabla p_{0h}, \bar{\boldsymbol{u}}_h) = (\boldsymbol{u}_0, \bar{\boldsymbol{u}}_h), & \text{(3.12a)} \\ (\nabla \cdot \boldsymbol{u}_{0h}, \bar{p}_h) + j(p_{0h}, \bar{p}_h) = 0 & \text{(3.12b)} \end{cases}$$

for all $(\bar{\boldsymbol{u}}_h, \bar{p}_h) \in \boldsymbol{V}_h \times P_h$.

In what follows we prove the existence and uniqueness of a solution to scheme (3.5)–(3.10). Since scheme (3.5)–(3.10) is a linear square finite-dimensional system (having the same number of unknowns as equations), uniqueness implies existence. Let $\delta\boldsymbol{d}_h^{n+1}$ and $\delta\boldsymbol{w}_h^{n+1}$ denote the difference between two possible solutions to (3.5). It is not hard to check that $\delta\boldsymbol{d}_h^{n+1}$ and $\delta\boldsymbol{w}_h^{n+1}$ satisfy

$$\begin{cases} \dfrac{1}{k}(\delta\boldsymbol{d}_h^{n+1}, \bar{\boldsymbol{w}}_h) + \lambda\, k((\nabla \boldsymbol{d}_h^n)^T \delta\boldsymbol{w}_h^{n+1}, (\nabla \boldsymbol{d}_h^n)^T \bar{\boldsymbol{w}}_h) + \gamma(\delta\boldsymbol{w}_h^{n+1}, \bar{\boldsymbol{w}}_h) = 0, & \text{(3.13a)} \\ (\nabla \delta\boldsymbol{d}_h^{n+1}, \nabla \bar{\boldsymbol{d}}_h) + \dfrac{H_F}{2\varepsilon^2}(\delta\boldsymbol{d}_h^{n+1}, \bar{\boldsymbol{d}}_h) - (\delta\boldsymbol{w}_h^{n+1}, \bar{\boldsymbol{d}}_h) = 0 & \text{(3.13b)} \end{cases}$$

for all $(\bar{\boldsymbol{d}}_h, \bar{\boldsymbol{w}}_h) \in \boldsymbol{D}_h \times \boldsymbol{W}_h$. Substituting $\bar{\boldsymbol{w}}_h = \delta\boldsymbol{w}_h^{n+1}$ and $\bar{\boldsymbol{d}}_h = \delta\boldsymbol{d}_h^{n+1}/k$ into (3.13a) and (3.13b), respectively, we have

$$\frac{1}{k}\|\nabla \delta\boldsymbol{d}_h^{n+1}\|^2 + \frac{H_F}{2k\varepsilon^2}\|\delta\boldsymbol{d}_h^{n+1}\|^2 + \gamma\|\delta\boldsymbol{w}_h^{n+1}\|^2 + \lambda k\|(\nabla \boldsymbol{d}_h^n)^T \delta\boldsymbol{w}_h^{n+1}\|^2 = 0.$$

This implies that $\delta\boldsymbol{w}_h^{n+1} = \boldsymbol{0}$ and $\delta\boldsymbol{d}_h^{n+1} = \boldsymbol{0}$. Thus we have proved uniqueness of a solution to (3.5). Analogously, we can prove the existence and uniqueness of a solution to (3.8) and (3.9).

4. A priori energy estimates. This section is devoted to proving a priori energy estimates for scheme (3.5)–(3.10). First, we prove that the potential approximation is stable owing to the additional term depending on H_F.

LEMMA 4.1. *It follows that*

$$\left(\boldsymbol{f}(\boldsymbol{d}_h^n)+\frac{H_F}{2}(\boldsymbol{d}_h^{n+1}-\boldsymbol{d}_h^n)\right)\cdot(\boldsymbol{d}_h^{n+1}-\boldsymbol{d}_h^n)\geq\Big(F(\boldsymbol{d}_h^{n+1})-F(\boldsymbol{d}_h^n)\Big) \tag{4.1}$$

holds, where $H_F>0$ is a bound of the L^∞-norm of the Hessian matrix associated to $F(\boldsymbol{d})$. For instance, $H_F=(M3^2+(M^2-M)2^2)^{1/2}$ as was defined in (3.7).

Proof. The Taylor expansion of $F(\boldsymbol{d})$ of order 1 with center $\boldsymbol{d}_h^n$ evaluated at $\boldsymbol{d}_h^{n+1}$ gives

$$\begin{aligned}F(\boldsymbol{d}^{n+1})-F(\boldsymbol{d}^n)&=\nabla_{\boldsymbol{d}}F(\boldsymbol{d}^n)\cdot(\boldsymbol{d}^{n+1}-\boldsymbol{d}^n)\\&\quad+\frac{1}{2}(\boldsymbol{d}^{n+1}-\boldsymbol{d}^n)^T H_{\boldsymbol{d}}F(\boldsymbol{d}^{n+\theta})(\boldsymbol{d}^{n+1}-\boldsymbol{d}^n),\end{aligned}$$

where $\boldsymbol{d}^{n+\theta}=\theta\boldsymbol{d}^{n+1}+(1-\theta)\boldsymbol{d}^n$ for some $\theta\in(0,1)$ and

$$H_{\boldsymbol{d}}F(\boldsymbol{d})_{ij}=\begin{cases}2d_id_j+(|\boldsymbol{d}|^2-1)\delta_{ij} & \text{if } |\boldsymbol{d}|\leq 1,\\ 2\dfrac{d_id_j}{|\boldsymbol{d}|^3}+2\dfrac{|\boldsymbol{d}|-1}{|\boldsymbol{d}|}\delta_{ij} & \text{if } |\boldsymbol{d}|>1\end{cases}$$

is the Hessian matrix of F with respect to $\boldsymbol{d}$. Since F is truncated to have quadratic growth at infinity, we obtain that $H_{\boldsymbol{d}}$ is uniformly bounded. In fact, we find that

$$\|H_{\boldsymbol{d}}F(\cdot)_{ij}\|_{L^\infty(\mathbb{R}^M)}\leq(2+\delta_{ij});$$

hence, the Frobenius norm is bounded by

$$\left(\sum_{i,j}^{M}\|H_{\boldsymbol{d}}F(\cdot)_{ij}\|^2_{L^\infty(\mathbb{R}^M)}\right)^{1/2}\leq H_F.$$

In particular,

$$\frac{1}{2}(\boldsymbol{d}^{n+1}-\boldsymbol{d}^n)^T H_{\boldsymbol{d}}F(\boldsymbol{d}^{n+\theta})(\boldsymbol{d}^{n+1}-\boldsymbol{d}^n)\leq\frac{H_F}{2}|\boldsymbol{d}^{n+1}-\boldsymbol{d}^n|^2. \tag{4.2}$$

Consequently, (4.1) is satisfied. ∎

Now, we are in a position to prove a local-in-time discrete energy law.

LEMMA 4.2. *Assume that hypotheses* (H1)–(H4) *hold. Then the solution* $(\boldsymbol{u}_h^{n+1}, p_h^{n+1}, \boldsymbol{d}_h^{n+1}, \boldsymbol{w}_h^{n+1})$ *to scheme* (3.5)–(3.10) *satisfies the inequality*

$$\mathcal{E}(\widetilde{\boldsymbol{u}}_h^{n+1},\boldsymbol{d}_h^{n+1})-\mathcal{E}(\widetilde{\boldsymbol{u}}_h^{n},\boldsymbol{d}_h^{n})+k\left(\nu\|\nabla\boldsymbol{u}_h^{n+1}\|^2+\lambda\gamma\|\boldsymbol{w}_h^{n+1}\|^2\right)\leq 0, \tag{4.3}$$

where $\mathcal{E}(\boldsymbol{u},\boldsymbol{d})$ is defined in (2.9) *and*

$$\widetilde{\boldsymbol{u}}_h^{n+1}=\boldsymbol{u}_h^{n+1}-k\nabla p_h^{n+1}. \tag{4.4}$$

Proof. We have, by using $\bar{p}_h=p_h^{n+1}$ as a test function in (3.9) and taking into account (4.4),

$$j(p_h^{n+1},p_h^{n+1})=(\boldsymbol{u}_h^{n+1}-k\nabla p_h^{n+1},\nabla p_h^{n+1})=(\widetilde{\boldsymbol{u}}_h^{n+1},\nabla p_h^{n+1}),$$

and hence we obtain, by squaring (4.4),

$$\frac{1}{2}\|\widetilde{\boldsymbol{u}}_h^{n+1}\|^2 - \frac{1}{2}\|\boldsymbol{u}_h^{n+1}\|^2 + \frac{k^2}{2}\|\nabla p_h^{n+1}\|^2 + k\, j(p_h^{n+1}, p_h^{n+1}) = 0.$$

Next, by substituting $\widehat{\boldsymbol{u}}_h$ given in (3.6) into (3.8) and selecting $\bar{\boldsymbol{u}}_h = k\,\boldsymbol{u}_h^{n+1}$ as a test function in (3.8), it follows that

$$\frac{1}{2}\|\boldsymbol{u}_h^{n+1}\|^2 - \frac{1}{2}\|\widehat{\boldsymbol{u}}_h\|^2 + \frac{1}{2}\|\boldsymbol{u}_h^{n+1} - \widehat{\boldsymbol{u}}_h\|^2 + \nu\, k\|\nabla \boldsymbol{u}_h^{n+1}\|^2 = 0.$$

By adding these last two equations, we find

$$\begin{aligned} &\tfrac{1}{2}\|\widetilde{\boldsymbol{u}}_h^{n+1}\|^2 - \tfrac{1}{2}\|\widehat{\boldsymbol{u}}_h\|^2 + \nu\, k\|\nabla \boldsymbol{u}_h^{n+1}\|^2 + \tfrac{1}{2}\|\boldsymbol{u}_h^{n+1} - \widehat{\boldsymbol{u}}_h\|^2 \\ &\quad + \tfrac{k^2}{2}\|\nabla p_h^{n+1}\|^2 + k\, j(p_h^{n+1}, p_h^{n+1}) = 0. \end{aligned} \tag{4.5}$$

Moreover, if we choose $\bar{\boldsymbol{w}}_h = \lambda\, k\, \boldsymbol{w}_h^{n+1}$ in (3.5a) jointly with $\bar{\boldsymbol{d}}_h = \lambda(\boldsymbol{d}_h^{n+1} - \boldsymbol{d}_h^n)$ in (3.5b), and take into account (4.1), we arrive at

$$\begin{aligned} &\frac{\lambda}{2}\left(\|\nabla \boldsymbol{d}_h^{n+1}\|^2 - \|\nabla \boldsymbol{d}_h^n\|^2 + \|\nabla(\boldsymbol{d}_h^{n+1} - \boldsymbol{d}_h^n)\|^2\right) + \lambda\,\gamma\, k\|\boldsymbol{w}_h^{n+1}\|^2 \\ &\quad + \frac{\lambda}{\varepsilon^2}\int_\Omega \Big(F(\boldsymbol{d}_h^{n+1}) - F(\boldsymbol{d}_h^n)\Big) + \lambda\, k((\widehat{\boldsymbol{u}}_h \cdot \nabla)\boldsymbol{d}_h^n, \boldsymbol{w}_h^{n+1}) \le 0. \end{aligned} \tag{4.6}$$

By testing (3.6) by $\widehat{\boldsymbol{u}}_h$, we have

$$\frac{1}{2}\|\widehat{\boldsymbol{u}}_h\|^2 - \frac{1}{2}\|\widetilde{\boldsymbol{u}}_h^n\|^2 + \frac{1}{2}\|\widehat{\boldsymbol{u}}_h - \widetilde{\boldsymbol{u}}_h^n\|^2 - \lambda\, k((\nabla \boldsymbol{d}_h^n)^T \boldsymbol{w}_h^{n+1}, \widehat{\boldsymbol{u}}_h) = 0.$$

This equality, together with (4.5), (4.6), and the fact that

$$-((\nabla \boldsymbol{d}_h^n)^T \boldsymbol{w}_h^{n+1}, \widehat{\boldsymbol{u}}_h) + ((\widehat{\boldsymbol{u}}_h \cdot \nabla)\boldsymbol{d}_h^n, \boldsymbol{w}_h^{n+1}) = 0,$$

implies that

$$\begin{aligned} &\mathcal{E}(\widetilde{\boldsymbol{u}}_h^{n+1}, \boldsymbol{d}_h^{n+1}) - \mathcal{E}(\widetilde{\boldsymbol{u}}_h^n, \boldsymbol{d}_h^n) + k(\nu\|\nabla \boldsymbol{u}_h^{n+1}\|^2 + \lambda\gamma\|\boldsymbol{w}_h^{n+1}\|^2) \\ &\quad + \frac{1}{2}\|\boldsymbol{u}_h^{n+1} - \widehat{\boldsymbol{u}}_h\|^2 + \frac{1}{2}\|\widehat{\boldsymbol{u}}_h - \widetilde{\boldsymbol{u}}_h^n\|^2 + \frac{\lambda}{2}\|\nabla(\boldsymbol{d}_h^{n+1} - \boldsymbol{d}_h^n)\|^2 + \frac{k^2}{2}\|\nabla p_h^{n+1}\|^2 \\ &\quad + k\, j(p_h^{n+1}, p_h^{n+1}) \le 0. \end{aligned}$$

This completes the proof. ∎

We are now ready to state the a priori global-in-time energy estimates for scheme (3.5)–(3.10). The proof follows easily from (4.3).

THEOREM 4.3. *Assume* (H1)–(H4). *The discrete solution* $\{(\boldsymbol{u}_h^n, \boldsymbol{d}_h^n, \boldsymbol{w}_h^{n+1})\}_{n=0}^N$ *of scheme* (3.5)–(3.10) *satisfies*

$$\max_{r\in\{0,\dots,N-1\}}\left\{\mathcal{E}(\boldsymbol{u}_h^{r+1}, \boldsymbol{d}_h^{r+1}) + k\sum_{n=0}^{r}\left(\nu\|\nabla \widetilde{\boldsymbol{u}}_h^{n+1}\|^2 + \lambda\gamma\|\boldsymbol{w}_h^{n+1}\|^2\right)\right\} \le \mathcal{E}(\boldsymbol{u}_{0h}, \boldsymbol{d}_{0h}). \tag{4.7}$$

In order to have a good initialization of scheme (3.5)–(3.10) we need the initial energy $\mathcal{E}(\boldsymbol{u}_{0h}, \boldsymbol{d}_{0h})$ to be bounded independent of (h, k, ε).

LEMMA 4.4. *Assume hypotheses* (H1)–(H4) *hold. If* (h, ε) *are chosen satisfying*

$$\frac{h}{\varepsilon} \leq K \tag{4.8}$$

for some constant $K > 0$*, then*

$$\mathcal{E}(\boldsymbol{u}_{0h}, \boldsymbol{d}_{0h}) \leq C_0 \tag{4.9}$$

for the initial approximations $(\boldsymbol{u}_{0h}, \boldsymbol{d}_{0h})$ *defined in* (3.11) *and* (3.12).

Proof. We use $\bar{\boldsymbol{u}} = \boldsymbol{u}_{0h}$ and $\bar{p}_h = p_{0h}$ as test functions in (3.12) to obtain

$$\frac{1}{2}\|\boldsymbol{u}_{0h}\|^2 + j(p_{0h}, p_{0h}) \leq \frac{1}{2}\|\boldsymbol{u}_0\|^2. \tag{4.10}$$

Moreover, from (3.4), we have

$$\|\boldsymbol{d}_{0h}\|_{\boldsymbol{H}^1(\Omega)} \leq C\|\boldsymbol{d}_0\|_{\boldsymbol{H}^1(\Omega)}. \tag{4.11}$$

Now, as in [18], we bound

$$\begin{aligned} \int_\Omega F(\boldsymbol{d}_{0h}) &\leq \int_\Omega (|\boldsymbol{d}_{0h}|^2 - |\boldsymbol{d}_0|^2)^2 = \int_\Omega (|\boldsymbol{d}_{0h} + \boldsymbol{d}_0||\boldsymbol{d}_{0h} - \boldsymbol{d}_0|)^2 \\ &\leq \|\boldsymbol{d}_{0h} + \boldsymbol{d}_0\|^2_{\boldsymbol{L}^\infty(\Omega)}\|\boldsymbol{d}_{0h} - \boldsymbol{d}_0\|^2 \leq C\, h^2\|\boldsymbol{d}_0\|^2_{\boldsymbol{H}^1(\Omega)}, \end{aligned} \tag{4.12}$$

where (3.3) and (3.2) have been applied. Combining (4.12) with (4.10) and (4.11) together with (4.8), we obtain (4.9). ∎

Remark 4.5. Hypothesis (4.8) is rarely explicitly mentioned in numerical papers based on algorithms using the penalty approach, but it is required to guarantee a priori energy estimates independent of ε. It seems that this condition is overlooked. Nevertheless, it is important to underline that the constraint (4.8) for (h, ε) comes only from the approximation of $\boldsymbol{d}_0$ in $\boldsymbol{D}_h$ but not from the discrete scheme itself.

Remark 4.6. In the present paper we have developed a time-splitting algorithm based on the nonincremental projection method, even though it could be applied to the incremental projection method with obvious modifications. For clarity of exposition, we have considered only the nonincremental approach since it involves fewer terms and requires a much easier initialization.

5. Numerical results. We present a reformulation of system (3.5) to avoid computing the auxiliary variable $\boldsymbol{w}_h^{n+1}$. Based on this reformulation, we will show some numerical experiments that illustrate the stability, accuracy, efficiency, and reliability of the scheme. In doing so, we first test our numerical approximation simulating annihilation of singularities. Next we will investigate the numerical accuracy with respect to time and space, in order to conclude that the splitting error does not deteriorate the convergence rate of the velocity and pressure from the nonincremental projection method for the Navier–Stokes equations [32, 34, 17]. Finally, we will check numerically the conditional stability which depends on the size of the stabilization constant H_F.

We take the approximating spaces $\boldsymbol{D}_h, \boldsymbol{V}_h$, and P_h described in (H3). The numerical solutions are implemented with the help of FreeFem++ [19].

5.1. Implementation strategy. It is clear that the computation of the auxiliary vector $\boldsymbol{w}_h^{n+1}$ in (3.5) gives rise to an important amount of computer memory and time in comparison with systems (3.8) and (3.9). Thus, scheme (3.5)–(3.8) will become much more efficient if we are able to remove $\boldsymbol{w}_h^{n+1}$ from (3.5).

Let $N_d = \dim(\boldsymbol{D}_h)$ and $N_w = \dim(\boldsymbol{W}_h)$, and let $\{\psi_i^d\}_{i=1}^{N_d}$ and $\{\psi_i^w\}_{i=1}^{N_w}$ be finite-element bases for $\boldsymbol{D}_h$ and $\boldsymbol{W}_h$, respectively, constructed from the local basis of X_h and Y_h, respectively. Thus, define the following matrices. For $\boldsymbol{W}_h$, we have

$$\mathsf{M}_{d,w} = \left(\int_\Omega \phi_i^d \cdot \phi_j^w\right), \quad \mathsf{C}_w = \left(\int_\Omega ((\nabla \boldsymbol{d}_h^n)^T \phi_i^w \cdot \nabla)\boldsymbol{d}_h^n \cdot \phi_j^w\right), \quad \mathsf{M}_w = \left(\int_\Omega \phi_i^w \cdot \phi_j^w\right).$$

For $\boldsymbol{D}_h$, we have

$$\mathsf{M}_d = \left(\int_\Omega \phi_i^d \cdot \phi_j^d\right), \quad \mathsf{M}_{w,d} = \left(\int_\Omega \phi_i^w \cdot \phi_j^d\right), \quad \mathsf{L}_d = \left(\int_\Omega \nabla\phi_i^d \cdot \nabla\phi_j^d\right).$$

Moreover, let us denote by $\mathsf{W} \in \mathbb{R}^{N_w}$ and $\mathsf{D} \in \mathbb{R}^{N_d}$ the coordinate vectors, with respect to the fixed bases, of the finite-element functions $\boldsymbol{w}_h \in \boldsymbol{W}_h$ and $\boldsymbol{d}_h \in \boldsymbol{D}_h$, respectively. Thus, we can rewrite system (3.5) as

$$\begin{cases} \dfrac{1}{k}\mathsf{M}_{d,w}\mathsf{D}^{n+1} + (\lambda k \mathsf{C}_w + \gamma \mathsf{M}_w)\,\mathsf{W}^{n+1} = \dfrac{1}{k}\mathsf{M}_{d,w}\mathsf{D}^n - \mathsf{F}_w, & \text{(5.1a)} \\ \mathsf{L}_d\mathsf{D}^{n+1} + \dfrac{H_F}{2\varepsilon^2}\mathsf{M}_d\mathsf{D}^{n+1} - \mathsf{M}_{w,d}\mathsf{W}^{n+1} = -\dfrac{1}{\varepsilon^2}\mathsf{F}, & \text{(5.1b)} \end{cases}$$

where $\mathsf{F}_w \in \mathbb{R}^{N_d}$ and $\mathsf{F} \in \mathbb{R}^{N_w}$ are defined, respectively, as

(5.2)
$$\mathsf{F}_w = \left(\int_\Omega ((\boldsymbol{u}_h^n - k\nabla p_h^n)\cdot\nabla)\boldsymbol{d}_h^n \cdot \psi_j^w\right) \quad \text{and} \quad \mathsf{F} = \left(\int_\Omega \left(-\frac{H_F}{2}\boldsymbol{d}_h^n + \boldsymbol{f}(\boldsymbol{d}_h^n)\right)\cdot\phi_j^d\right).$$

From (5.1a), we have

$$\mathsf{W}^{n+1} = \mathsf{E}_w^{-1}\left[\frac{1}{k}\mathsf{M}_{d,w}\left(\mathsf{D}^n - \mathsf{D}^{n+1}\right) - \mathsf{F}_w\right],$$

where $\mathsf{E}_w = \lambda k \mathsf{C}_w + \gamma \mathsf{M}_w$ can be seen in two different ways depending on the reordering of the degrees of freedom of W^{n+1}: (1) a block-diagonal M-by-M matrix, which is easy to invert by using a block Gauss–Jordan elimination, or (2) an M-by-M block-diagonal matrix, since the degrees of freedom of two different elements are not coupled, which is also easily invertible by using block computations. The first approach is much more adequate especially for legacy code bases, which is our case here.

If we now replace the above equality in equations (5.1b), after some simple calculations, the resulting algorithm reads as

$$\left(\mathsf{L}_d + \frac{1}{k}\mathsf{M}_{w,d}\mathsf{E}_w^{-1}\mathsf{M}_{d,w} + \frac{H_F}{2\varepsilon^2}\mathsf{M}_d\right)\mathsf{D}^{n+1} = \mathsf{M}_{w,d}\mathsf{E}_w^{-1}\left[\frac{1}{k}\mathsf{M}_{d,w}\mathsf{D}^n - \mathsf{F}_w\right] - \frac{1}{\varepsilon^2}\mathsf{F}.$$

Observe that the matrix $\mathsf{L}_d + \frac{1}{k}\mathsf{M}_{w,d}\mathsf{E}_w^{-1}\mathsf{M}_{d,w} + \frac{H_F}{2\varepsilon^2}\mathsf{M}_d$ is the Schur complement of system (5.1) with respect to E_w.

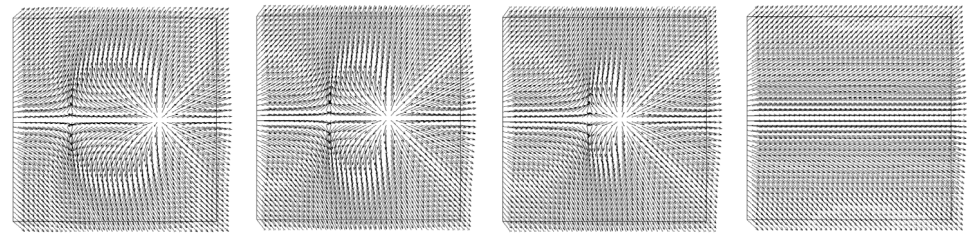

(a) $\|\boldsymbol{d}\|_\infty = 0.9962212$. (b) $\|\boldsymbol{d}\|_\infty = 0.9975724$. (c) $\|\boldsymbol{d}\|_\infty = 0.9960688$. (d) $\|\boldsymbol{d}\|_\infty = 0.9981066$.

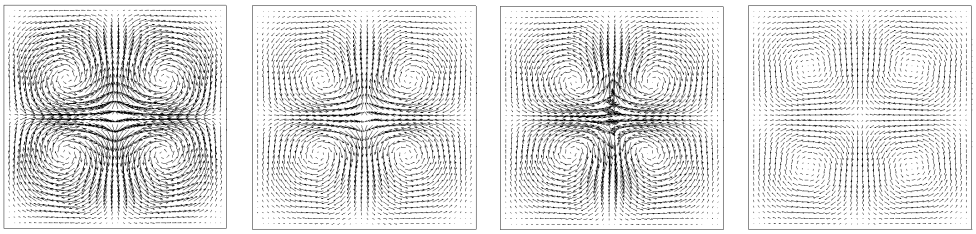

(e) $\|\boldsymbol{v}\|_\infty = 0.1220603$. (f) $\|\boldsymbol{v}\|_\infty = 0.07930149$. (g) $\|\boldsymbol{v}\|_\infty = 0.1052532$. (h) $\|\boldsymbol{v}\|_\infty = 0.00276648$.

FIG. 1. *Evolution of the director field* (a)–(d) *and velocity field* (e)–(h) *for the annihilation of two singularities at times* $t = 0.1$, 0.4, 0.6, *and* 1.

5.2. Annihilation. This numerical example is concerned with the phenomenon of annihilation of singularities. We will consider two numerical experiences consisting of the motion of two and four singularities. We will show the behavior of the energies, the singularities, and the velocity fields for each of these simulations.

The phenomenon of annihilation for two singularities was originally proposed in [28] for a Dirichlet boundary condition for the director field and also performed in [6] for a Neumann boundary condition as considered herein. It is computed on the domain $\Omega = (-1, 1) \times (-1, 1)$ with the initial conditions being

$$\boldsymbol{u}_0 = \boldsymbol{0}, \quad \boldsymbol{d}_0 = \frac{\tilde{\boldsymbol{d}}}{\sqrt{|\tilde{\boldsymbol{d}}|^2 + \varepsilon^2}}, \text{ where } \tilde{\boldsymbol{d}} = (x^2 + y^2 - 0.25, y),$$

and the physical parameters being $\nu = \lambda = \gamma = 1$. The discretization and penalization parameters are set as $(k, h, \varepsilon) = (0.001, 0.068986, 0.05)$. In Figure 1, we present snapshots of the director and velocity fields displayed at times $t = 0.1$, 0.4, 0.6, and 1. One can see how the two singularities are carried to the origin by the velocity field forming four vortices. The evolution of kinetic, elastic, and penalization energies, as well as the total energy, is depicted in Figure 2. Observe that the total energy decreases after each iteration as predicted by inequality (4.3). Moreover, the kinetic energy reaches its maximum level at the annihilation time. These numerical results are in good qualitative agreement with those obtained in [6].

For the annihilation of four singularities a zero initial velocity field $\boldsymbol{u}_0 = 0$ is also set as before, and the initial director field is considered as follows:

$$\boldsymbol{d}_0 = \frac{\tilde{\boldsymbol{d}}}{\sqrt{|\tilde{\boldsymbol{d}}|^2 + \varepsilon^2}}, \quad \text{where } \tilde{\boldsymbol{d}} = \left(\frac{x^2}{a^2} + \frac{y^2}{b^2} - 1, -xy\right),$$

where $a = 0.5$ and $b = 0.25$. Observe that the initial director field has two singularities

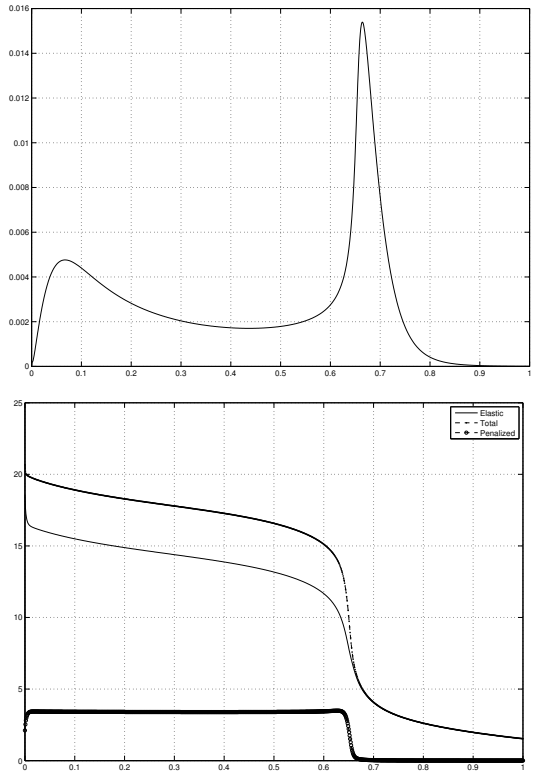

FIG. 2. *Evolution in time of the energies for the experiment of two singularities. Kinetic energy (top) and total, elastic, and penalization energies (bottom).*

at $(\pm 0.5, 0)$ and two more at $(0, \pm 0.25)$. The physical domain and parameters are the same as for the example with two singularities.

Contrary to what one might think at first sight, the four singularities mutually annihilate each other at the same time despite the fact that they are not at the same distance from the origin. To be more precise, the singularities at $(\pm 0.5, 0)$ start advancing toward the origin, while the ones at $(0, \pm 0.25)$ remain without moving, as depicted in Figure 3. This happens until the four singularities are equally spaced on a circle centered at the origin. Then the four singularities move together to the origin until disappearing at the same time. This is due to the fact that the velocity field in Figure 3 prevents the singularities at $(0, \pm 0.25)$ from moving toward each other while making the singularities at $(\pm 0.5, 0)$ get closer and closer to each other.

Concerning the evolution of the energy, note that the annihilation time $T_A = 0.14$ (see bottom image in Figure 4) does not occur at the maximum value of the kinetic energy $T_{kin} = 0.04$ (see top image in Figure 4). The total and elastic energies decrease, and the penalty energy increases at the beginning of the simulation and then decreases as shown in the bottom image of Figure 4.

5.3. Convergence rate. We are now interested in the accuracy with respect to time and space. For this, we are going to use the experimental order of convergence method, considering $\Omega = (0, 1) \times (-\frac{1}{2}, \frac{1}{2})$, $\lambda = \gamma = \nu = 1$, and $\varepsilon = 0.05$. The initial

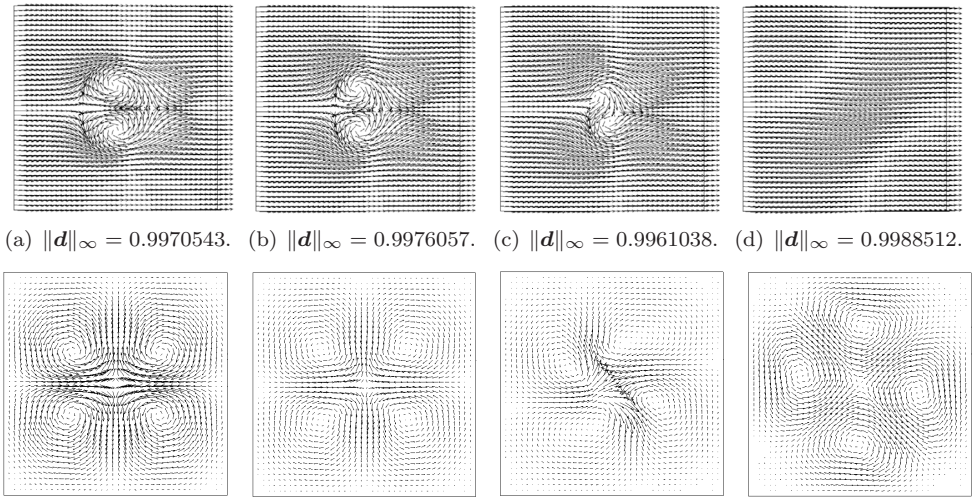

(a) $\|\boldsymbol{d}\|_\infty = 0.9970543$. (b) $\|\boldsymbol{d}\|_\infty = 0.9976057$. (c) $\|\boldsymbol{d}\|_\infty = 0.9961038$. (d) $\|\boldsymbol{d}\|_\infty = 0.9988512$.

(e) $\|\boldsymbol{v}\|_\infty = 0.1220603$. (f) $\|\boldsymbol{v}\|_\infty = 0.07930149$. (g) $\|\boldsymbol{v}\|_\infty = 0.1052532$. (h) $\|\boldsymbol{v}\|_\infty = 0.00276648$.

FIG. 3. *Evolution of the director field* (a)–(d) *and velocity field* (e)–(h) *for the annihilation of four singularities at times* $t = 0.05$, 0.1, 0.14, *and* 0.25.

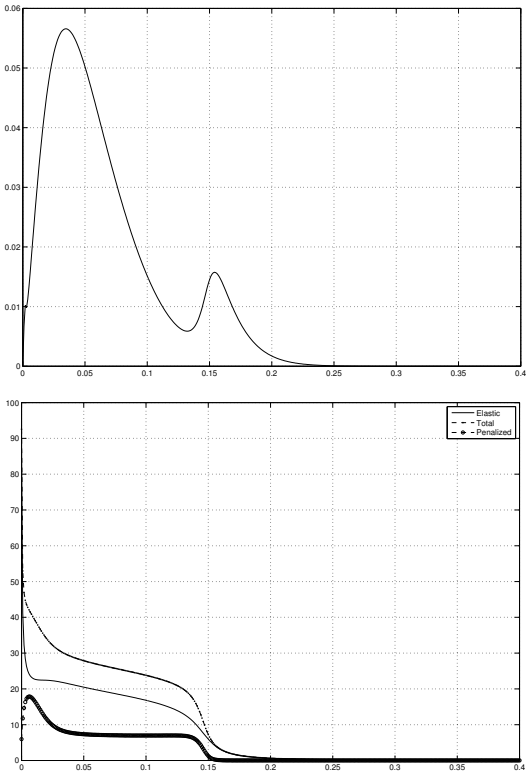

FIG. 4. *Evolution in time of the energies for the annihilation of four singularities. Kinetic energy (top) and total, elastic, and penalization energies (bottom).*

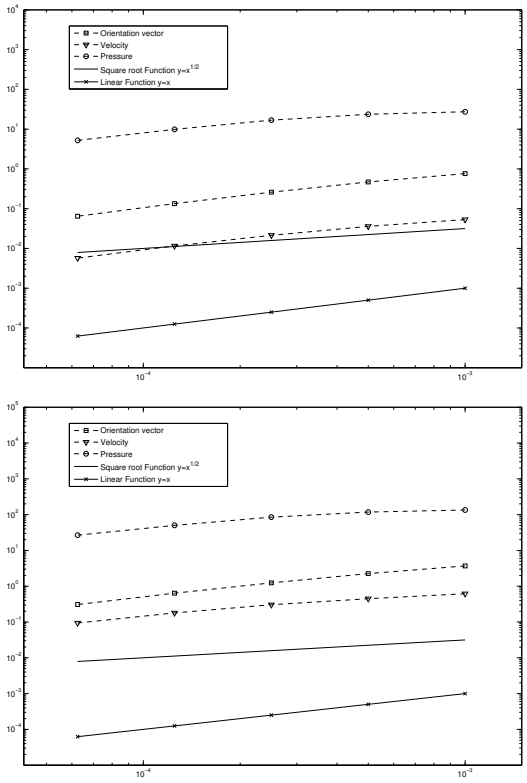

FIG. 5. *Behavior of the time error in the $L^2(\Omega)$-norm (top) and the $H^1(\Omega)$-norm (bottom) for the director, velocity, and pressure fields.*

TABLE 1
The time convergence rates for the velocity, pressure, and director fields.

k	L^2-rate-p	$\boldsymbol{L}^2$-rate-$\boldsymbol{v}$	$\boldsymbol{L}^2$-rate-$\boldsymbol{d}$	H^1-rate-p	$\boldsymbol{H}^1$-rate-$\boldsymbol{v}$	$\boldsymbol{H}^1$-rate-$\boldsymbol{d}$
10^{-3}	–	–	–	–	–	–
$5 \cdot 10^{-4}$	0.2115	0.5686	0.6989	0.1951	0.4600	0.7158
$2.5 \cdot 10^{-4}$	0.4910	0.7478	0.8513	0.4689	0.5559	0.8572
$1.25 \cdot 10^{-4}$	0.7699	0.8897	0.9579	0.7657	0.7631	0.9596
$6.25 \cdot 10^{-5}$	0.9173	1.0142	1.0542	0.9065	0.9355	1.0545

data are taken as

$$\boldsymbol{u}_0 = \boldsymbol{0} \quad \text{and} \quad \boldsymbol{d}_0 = (\sin(a), \cos(a)), \quad \text{where } a = \pi(\cos(\pi x) + \sin(\pi y)).$$

which satisfies homogeneous Dirichlet conditions for the velocity field and homogeneous Neumann boundary conditions for the director field.

To measure the time error, the reference solution is taken as the numerical approximation computed on the discrete parameters $(k, h) = (1.5625e10^{-6}, 0.068986)$. In Figure 5 and Table 1, we illustrate the time error behavior and the convergence rate for the director, velocity, and pressure fields measured in the $L^2(\Omega)$- and $H^1(\Omega)$-norms

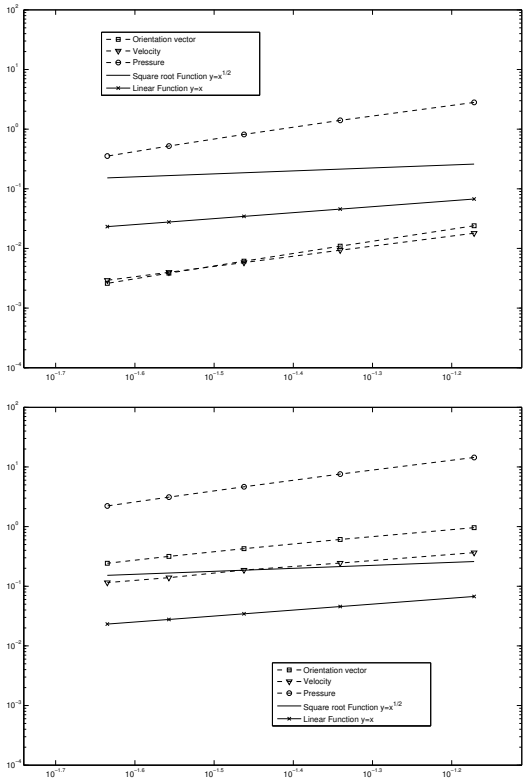

FIG. 6. *Behavior of the space error in the $L^2(\Omega)$-norm (top) and the $H^1(\Omega)$-norm (bottom) for the director, velocity, and pressure fields.*

for several time steps. The tests have been performed by comparing our reference solution with the numerical approximation computed on five time steps $k_{i+1} = 0.5k_i$ for $i = 1, 2, 3, 4$ with $k_1 = 10^{-3}$. We approach $\mathcal{O}(k)$ in the $\boldsymbol{L}^2(\Omega)$-norm for the velocity and director vector, which is consistent with the results for the velocity in the context of the nonincremental projection method for the Navier–Stokes equations. The error for the director field in the $\boldsymbol{H}^1(\Omega)$-norm is of $\mathcal{O}(k)$, which means the splitting error associated to the segregation has no influence on the order of the director. Instead, the error for the velocity field in the $\boldsymbol{H}^1(\Omega)$-norm does not maintain the first-order accuracy, which could mean that the order of the segregation will be less than first order. Furthermore, the error for the pressure in the $L^2(\Omega)$- and $H^1(\Omega)$-norms behaves as that for the velocity for the $H^1(\Omega)$-norm.

With respect to the space error behavior, we compute the reference solution on $(h, k) = (0.0083, 0.001)$. The corresponding approximate errors, defined as the difference with this reference solution, is performed for $h = 0.0673$, 0.0456, 0.0345, 0.0277, and 0.0232. In Figure 6 and Table 2, we show the spatial convergence rate on the director, velocity, and pressure fields measured in the $L^2(\Omega)$- and $H^1(\Omega)$-norms for several mesh sizes. The velocity and director errors in the $L^2(\Omega)$- and $H^1(\Omega)$-norms are of $\mathcal{O}(h^{1.5})$ and $\mathcal{O}(h)$, and $\mathcal{O}(h^2)$ and $\mathcal{O}(h^{1.5})$, respectively, and the pressure errors in the $L^2(\Omega)$- and $H^1(\Omega)$-norms are of $\mathcal{O}(h^2)$ and $\mathcal{O}(h^{1.5})$. It is rather surprising that the accuracy for the pressure is better than that for the velocity, although the absolute errors for the velocity are lower than those for the pressure; see Figure 6.

TABLE 2
The space convergence rates for the velocity, pressure, and director fields.

h	L^2-rate-p	$\boldsymbol{L}^2$-rate-$\boldsymbol{v}$	$\boldsymbol{L}^2$-rate-$\boldsymbol{d}$	H^1-rate-p	$\boldsymbol{H}^1$-rate-$\boldsymbol{v}$	$\boldsymbol{H}^1$-rate-$\boldsymbol{d}$
0.0673	–	–	–	–	–	–
0.0456	1.7761	1.6878	2.0255	1.6420	1.0313	1.1675
0.0345	1.9376	1.7025	2.0688	1.7667	0.9731	1.2747
0.0277	2.0554	1.7212	2.1841	1.8265	1.3396	1.3637
0.0232	2.1681	1.7269	2.2921	1.8875	1.0663	1.4823

TABLE 3
Stability dependence of scheme (3.5)–(3.10) *on the parameters* M *and* ε *for the annihilation phenomenon with two singularities.* T_A *is the annihilation time.*

$\varepsilon \backslash M$	0	0.5	1	1.5	2	
0.1	✓ 0.215 0.01670914	✓ 0.235 0.01443464	✓ 0.247 0.01328788	✓ 0.258 0.01233513	✓ 0.269 0.01150359	Stab. T_A E_{kin}
0.05	✓ 0.327 0.04200973	✓ 0.451 0.02695581	✓ 0.526 0.02166554	✓ 0.596 0.01806961	✓ 0.664 0.01539423	Stab. T_A E_{kin}
0.01	✗ –– ––	✓ **No annihil.** 0.003715506	✓ **No annihil.** 0.001635032	✓ **No annihil.** 0.0009440176	✓ **No annihil.** 0.0006196211	Stab. T_A E_{kin}
0.001	✗ –– ––	✓ **No annihil.** 0.006349918	✓ **No annihil.** 0.002473232	✓ **No annihil.** 0.00134994	✓ **No annihil.** 0.0008570226	Stab. T_A E_{kin}

5.3.1. Dependence of the stability on the constant H_F. Next we want to study the sensitivity of scheme (3.5)–(3.10) with respect to the stabilization constant H_F given in (3.7), which depends on the space dimension M in an increasing manner and on the penalty parameter ε. In doing so, we will consider the phenomenon of annihilation of two singularities described above for fixed $(h, k) = (0.068986, 0.001)$ and varying (ε, M) in the range $\varepsilon = 0.1$, 0.05, 0.01, and 0.001 and $M = 0$, 0.5, 1, 1.5, and 2. The annihilation times T_A reported in Table 3 are taken as those times where the value of the kinetic energy is maximum. For these values, we observe that scheme (3.5)–(3.10) is unconditionally stable for $M \geq 0.5$ and conditionally stable for $M = 0$, because strong spurious oscillations appear for $\varepsilon = 0.01$ and 0.001. In particular, for $M = 0$, it can be proved by following the analysis performed in [18] that a relation among (k, h, ε) must be small enough in order to get energy stability. Moreover, for $\varepsilon = 0.1$ and 0.05, the annihilation time becomes smaller and smaller as M decreases to 0, and the maximum of the kinetic energy decreases as H_F becomes bigger and bigger. But the qualitative behavior remains the same. However, this situation changes drastically as ε takes the values 0.01 and 0.001 where there is no longer annihilation (see Figure 7). A possible explanation of this fact might be that the velocity field produced via the elastic tensor is not enough to move the defect points through the convective term in the director equation. In particular, observe that the kinetic energy for $\varepsilon = 0.01$ and 0.001 decays practically to zero from the beginning. In light of the above, one might think that if the kinetic energy associated to a velocity field was large enough to move the singularities, then they would move each other.

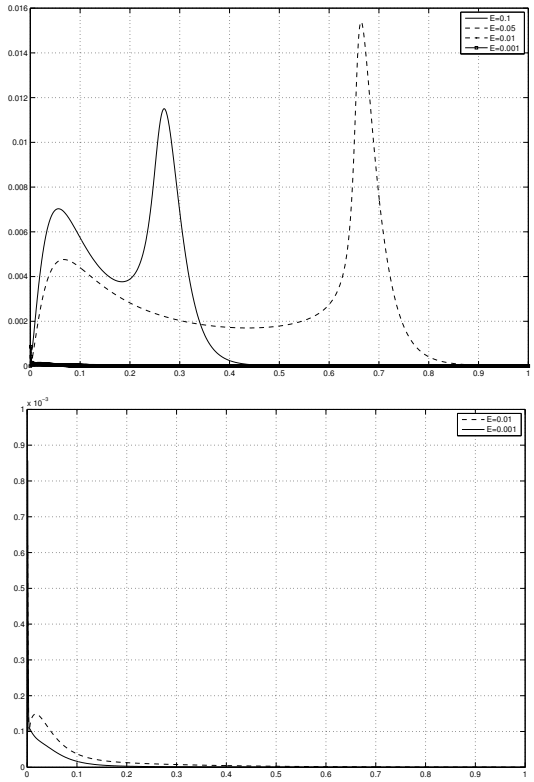

FIG. 7. *The time evolution of the kinetic energy for* $\varepsilon = 0.1, 0.05, 0.01, 0.001$ *for two singularities (top). Since the maximum values of the kinetic energy for* $\varepsilon = 0.01, 0.001$ *are* $6.1962 \cdot 10^{-4}$ *and* $8.5702 \cdot 10^{-4}$*, respectively, we include these separately (bottom).*

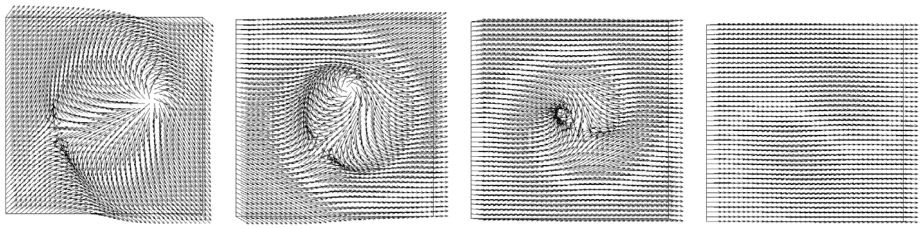

(a) $\|\boldsymbol{d}\|_\infty = 1.068284$. (b) $\|\boldsymbol{d}\|_\infty = 1.036288$. (c) $\|\boldsymbol{d}\|_\infty = 1.031044$. (d) $\|\boldsymbol{d}\|_\infty = 1.000078$.

FIG. 8. *Evolution of the director field for a rotating flow at times* $t = 0.5, 2.5, 5.5,$ *and* 8.

In order to corroborate the above statement, we will consider an initial and boundary velocity corresponding to a rotating flow of the form $\boldsymbol{u} = \omega(-y, x)^T$ with $\omega = 100$. We must point out that the rotating flow does not carry the singularities to be closer to each other. They might be rotating continuously without annihilating. The parameters are selected as $(k, h, \varepsilon) = (0.001, 0.068986, 0.01)$. In Figure 8, we plot the director field at four different times: at $t = 0.05$, where the singularities are swirled around with the flow; at $t = 2.5$, where the singularities keep on moving closer and closer to each other with the flow; at $t = 5.5$, with the singularities just prior to annihilation; and, finally, at $t = 8$, where a equilibrium solution is reached.

Thus we can conclude that the velocity field plays an important role in the annihilation of singularities. It seems that there exists a relation between the amount of the kinetic energy and the size of the penalty parameter ε that makes the singularities move. Moreover, the fact that the singularities disappear is due to their opposite signs; otherwise, they would move apart toward a steady state solution determined by the boundary conditions.

6. Conclusions. In this paper a time-splitting numerical algorithm based on the Chorin–Temam projection method has been proposed for approximating the Ericksen–Leslie equations, where a variant of the Ginzburg–Laundau penalization for approximating the sphere constraint has been considered. To the best of our knowledge, the algorithm proposed herein is the first one that is linear and unconditionally stable. The key ingredient for this is to introduce an adequate numerical dissipation depending on a first-order Taylor approximation for the penalty function $F(\boldsymbol{d})$. Another key feature is that this algorithm does not require introducing any auxiliary variable in the director problem (at the algebraic level) and allows equal-order interpolation for all the unknowns, in particular, for the velocity and pressure.

We have carried out several numerical experiments of annihilation of singularities so that our method can be compared with existing methods. In particular, the results of the annihilation phenomenon of two singularities fits pretty well with those reported in [6] and [3]. Furthermore, we have checked the numerical accuracy in time and space. Concerning the time error behavior, the results indicate that the splitting error is first-order in accordance with those for the Chorin–Temam projection method. It is worth noting that we have obtained interesting results for small ε for the two singularities problem, establishing a relation between the kinetic energy and the annihilation of singularities from the numerical point of view. This has been possible due to the condition number of the linear system seeming to be less dependent on ε than for other methods. The only method with the same feature in the literature is the one using a saddle-point approach [3], but it is fully coupled. Therefore, our method is more efficient since it involves less computational work. Moreover, we have observed in Table 3 that the annihilation time and the kinetic energy value are modified via the value of H_F, but qualitatively the numerical solutions are the same.

REFERENCES

[1] F. Armero and J. C. Simo, *Formulation of a new class of fractional-step methods for the incompressible MHD equations that retains the long-term dissipativity of the continuum dynamical system*, in Integration Algorithms and Classical Mechanics, Fields Inst. Commun. 10, AMS, Providence, RI, 1996, pp. 1–23.

[2] S. Badia, *On stabilized finite element methods based on the Scott-Zhang projector. Circumventing the inf-sup condition for the Stokes problem*, Comput. Methods Appl. Mech. Engrg., 247/248 (2012), pp. 65–72.

[3] S. Badia, F. Guillén-Gonzalez, and J. V. Gutiérrez-Santacreu, *Finite element approximation of nematic liquid crystal flows using a saddle-point structure*, J. Comput. Phys., 230 (2011), pp. 1686–1706.

[4] S. Badia, F. Guillén-Gonzalez, and J. V. Gutiérrez-Santacreu, *An overview on numerical analyses of nematic liquid crystal flows*, Arch. Comput. Methods Engrg., 18 (2011), pp. 285–313.

[5] S. Badia, R. Planas, and J. V. Gutiérrez-Santacreu, *Unconditionally stable operator splitting algorithms for the incompressible magnetohydrodynamics system discretized by a stabilized finite element formulation based on projections*, Internat. J. Numer. Methods Engrg., 93 (2013), pp. 302–328.

[6] R. Becker, X. Feng, and A. Prohl, *Finite element approximations of the Ericksen–Leslie model for nematic liquid crystal flow*, SIAM J. Numer. Anal., 46 (2008), pp. 1704–1731.

[7] S. C. Brenner and L. R. Scott, *The Mathematical Theory of Finite Element Methods*, Texts Appl. Math. 15, Springer-Verlag, Berlin, 1994.
[8] E. Burman and M. A. Fernández, *Galerkin finite element methods with symmetric pressure stabilization for the transient Stokes equations: Stability and convergence analysis*, SIAM J. Numer. Anal., 47 (2008), pp. 409–439.
[9] A. J. Chorin, *Numerical solution of the Navier-Stokes equations*, Math. Comp., 22 (1968), pp. 745–762.
[10] P. G. de Gennes and J. Prost, *The Physics of Liquid Crystals*, 2nd ed., Oxford Science Publications, Oxford, UK, 1993.
[11] C. L. Dohrmann and P. B. Bochev, *A stabilized finite element method for the Stokes problem based on polynomial pressure projections*, Internat. J. Numer. Methods Fluids, 46 (2004), pp. 183–201.
[12] J. Ericksen, *Conservation laws for liquid crystals*, Trans. Soc. Rheology, 5 (1961), pp. 22–34.
[13] J. Ericksen, *Continuum theory of nematic liquid crystals*, Res. Mechanica, 21 (1987), pp. 381–392.
[14] J. L. Ericksen, *Liquid crystals with variable degree of orientation*, Arch. Rational Mech. Anal., 113 (1990), pp. 97–120.
[15] F. C. Frank, *On the theory of liquid crystals*, Discuss. Faraday Soc., 25 (1958), pp. 19–28.
[16] V. Girault and F. Guillén-González, *Mixed formulation, approximation and decoupling algorithm for a penalized nematic liquid crystals model*, Math. Comp., 80 (2011), pp. 781–819.
[17] J.-L. Guermond, P. Minev, and J. Shen, *An overview of projection methods for incompressible flows*, Comput. Methods Appl. Mech. Engrg., 195 (2006), pp. 6011–6045.
[18] F. M. Guillén-Gonzalez and J. V. Gutiérrez-Santacreu, *A linear mixed finite element scheme for a nematic Ericksen-Leslie liquid crystal model*, ESAIM Math. Model. Numer. Anal., 47 (2013), pp. 1433–1464.
[19] F. Hecht, *New development in freefem++*, J. Numer. Math., 20 (2012), pp. 251–265.
[20] Q. Hu, X.-C. Tai, and R. Winther, *A saddle point approach to the computation of harmonic maps*, SIAM J. Numer. Anal., 47 (2009), pp. 1500–1523.
[21] F. Leslie, *Some constitutive equations for liquid crystals*, Arch. Rational Mech. Anal., 28 (1968), pp. 265–283.
[22] F. Leslie, *Theory of flow phenomena in liquid crystals*, in Advances in Liquid Crystals, Vol. 4, G. H. Brown, ed., Academic Press, New York, 1979, pp. 1–81.
[23] F. H. Lin, *Nonlinear theory of defects in nematic liquid crystals: Phase transition and flow phenomena*, Comm. Pure Appl. Math., 42 (1989), pp. 789–814.
[24] F. H. Lin and C. Liu, *Non-parabolic dissipative systems modelling the flow of liquid crystals*, Comm. Pure Appl. Math., 48 (1995), pp. 501–537.
[25] F. H. Lin and C. Liu, *Static and dynamic theories of liquid crystals*, J. Partial Differential Equations, 14 (2001), pp. 289–330.
[26] P. Lin and C. Liu, *Simulations of singularity dynamics in liquid crystal flows: A C^0 finite element approach*, J. Comput. Phys., 215 (2006), pp. 1411–1427.
[27] P. Lin, C. Liu, and H. Zhang, *An energy law preserving C^0 finite element scheme for simulating the kinematic effects in liquid crystal flow dynamics*, J. Comput. Phys., 227 (2007), pp. 348–362.
[28] C. Liu and N. J. Walkington, *Approximation of liquid crystal flows*, SIAM J. Numer. Anal., 37 (2000), pp. 725–741.
[29] C. Liu and N. J. Walkington, *Mixed methods for the approximation of liquid crystal flows*, M2AN Math. Model. Numer. Anal., 36 (2002), pp. 205–222.
[30] S. Minjeaud, *An unconditionally stable uncoupled scheme for a triphasic Cahn-Hilliard/Navier-Stokes model*, Numer. Methods Partial Differential Equations, 29 (2013), pp. 584–618.
[31] C. Oseen, *The theory of liquid crystals*, Trans. Faraday Soc., 29 (1933), pp. 883–899.
[32] R. Rannacher, *On Chorin's projection method for the incompressible Navier-Stokes equations*, in The Navier-Stokes Equations II—Theory and Numerical Methods (Oberwolfach, 1991), Lecture Notes in Math. 1530, Springer, Berlin, 1992, pp. 167–183.
[33] L. R. Scott and S. Zhang, *Finite element interpolation of non-smooth functions satisfying boundary conditions*, Math. Comp., 54 (1990), pp. 483–493.
[34] J. Shen, *On error estimates of projection methods for Navier–Stokes equations: First-order schemes*, SIAM J. Numer. Anal., 29 (1992), pp. 57–77.
[35] R. Temam, *Sur l'approximation de la solution des équations de Navier-Stokes par la méthode des pas fractionnaires*, Arch. Rational Mech. Anal., 33 (1969), pp. 377–385.
[36] R. Temam, *Navier-Stokes Equations, Theory and Numerical Analysis*, North-Holland, Amsterdam, 1979.